Uniaxial phase of alkali metals on a fcc (100) metal surface

Neil D. Shrimpton
Department of Chemistry, Pennsylvania State University, University Park, Pennsylvania 16802

Gail S. Welsh and Jinsuk Song
Department of Physics, Pennsylvania State University, University Park, Pennsylvania 16802
(Received 14 June 1991)

The overlayer phases of alkali metals on a fcc (100) surface are modeled by simple dipole moment interactors on a modulated potential surface. Ground-state configurations are determined, and the criteria are established under which a uniaxial phase can be formed. The effect of lateral variation in the substrate potential on the structure of the uniaxial phase is examined. Scattering profiles are calculated and we show how they are influenced by this substrate corrugation. Domain-wall pinning and thermal influences are also considered.

I. INTRODUCTION

Alkali-metal adsorption on metal surfaces has been the subject of considerable study going back to the work of Langmuir in the 1920s. From scattering studies, it is found that the adsorbed alkali-metal atoms form a great variety of structures on the metal substrates.[1,2]

Upon adsorption, there is a significant shift of electron density from the alkali-metal atoms towards the adsorbing surface.[3] A large dipole moment p can be associated with each alkali-metal atom, regardless of whether there is actual charge transfer to the substrate or just an atomic polarization.[4,5] The dipole moment leads to a repulsive interaction potential of $2p^2/r^3$ between alkali-metal atoms on the metal surface. The dipole moments are known to be several Debye in magnitude,[6,7] so at typical nearest-neighbor distances this potential can approach a few tenths of an eV. Consequently, there is a significant force of repulsion between atoms.

This dipole moment does vary with the coverage of alkali-metal atoms.[8] The electric field exerted by one alkali-metal atom will depolarize its neighbors.[9] At close distances, where there is overlap of electron wave functions, this simple depolarization process is made more complex by metallization. With increased coverage the dipole interaction is reduced in magnitude, and orbital overlap leads to direct alkali-metal atom metallic bonding. The point at which metallization becomes apparent is identified by a minimum in the work function with coverage.[10] Other possible interactions between the alkali-metal atoms have been reviewed by Einstein.[11] The consequences of such interactions on the structures formed in alkali-metal overlayers has been reviewed by Naumovets,[12] with the conclusion that the dipole interaction dominates all other interactions between adatoms.

The substrate interaction is not uniform across the surface of the substrate, leading to energetically preferred adsorption sites. This variation need not be significant, as has been indicated by density-functional calculations on normal metal surfaces.[13] A variation in the potential can be expected from core repulsions with the substrate atoms. With transition-metal substrates, the substrate atom d orbital electrons leads to localized interactions with the alkali-metal atoms[14] and hence a large potential variation across the substrate. At present, very little is known about the magnitude of the substrate potential variation.

It is clear from the number of commensurate phases that occur with alkali-metal adsorption that the substrate variation, otherwise known as the corrugation, cannot be neglected. However, there are many phases that are incommensurate with the substrate. There is an interplay between alkali-alkali interactions and alkali-substrate interactions that determines the structure of these phases. In the case of alkali metals on nonrefractory transition-metal surfaces, the incommensurate phases exhibit a uni-

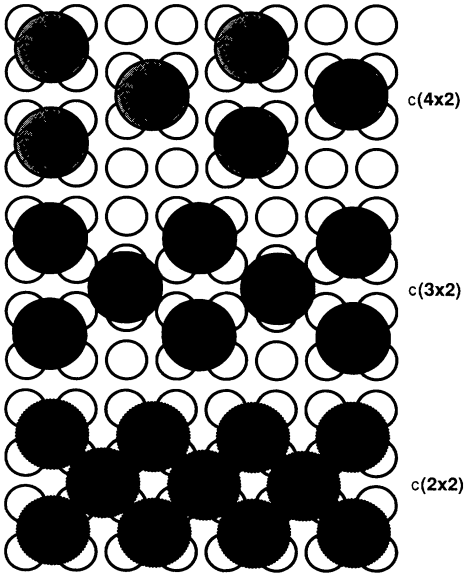

FIG. 1. The $c(4\times2)$, $c(3\times2)$, and $c(2\times2)$ commensurate phases.

form spacing of the alkali-metal atoms. For such systems it is clear that the dipole interaction almost entirely determines the structure, with the substrate interaction only becoming evident at densities which favor the formation of a commensurate phase.[1]

It is such systems, where the dipole interaction of the adatoms dominates the lateral interaction of the substrate, that we focus on in this study. To leading order, the (100) face of the metal substrate provides an interaction potential with a particularly simple parametrization

$$V(x,y,z)=V_0(z)-2V_g(z)[\sin(2\pi x/a_0)+\sin(2\pi y/a_0)]\ , \quad (1)$$

where $V_0(z)$ is the averaged holding potential of the substrate, $V_g(z)$ is known as the substrate corrugation, and a_0 is the spacing between substrate atoms. A uniaxial phase occurs between the $c(4\times2)$ and $c(3\times2)$ commensurate densities. The structure of these phases is given in Fig. 1. It is this uniaxial phase that will be the subject of our study.

II. CALCULATION

With the dipole interaction between alkali-metal atoms, and with the substrate interaction of (1), the total energy of N adsorbed atoms is

$$E=\sum_{\mathbf{r}_i,\mathbf{r}_j}\frac{p^2}{|\mathbf{r}_i-\mathbf{r}_j|^3}+NV_0-\sum_{\mathbf{r}_i}2V_g[\sin(2\pi x/a_0)+\sin(2\pi y/a_0)]\ . \quad (2)$$

$\mathbf{r}_i$ and $\mathbf{r}_j$ are positions of the atoms along the surface, and the assumption is made that any nonuniformity in the heights of the adatoms is insignificant compared to the interalkali-metal spacings. V_0 being constant in (2) does not influence the positioning of the adatoms and can be neglected. If V_g is factored from (2), and if all length scales are expressed in terms of the substrate spacing a_0, only one parameter remains, $2p^2/V_g a_0^3$, which we label c.

The value of c depends on the relative strength of the dipole interaction of the substrate corrugation. As an example, for K on Ni(100) in the density range of interest, a reasonable value for p is 5 Debye. With the Ni(100) substrate spacing of 2.49 Å, this gives a value $p^2/a_0^3=1.00$ eV. Estimates of substrate corrugation for Ni(111) place an upper limit of 0.05 eV on the total substrate potential variation, and the suggestion is made that the actual corrugation may be substantially less than this.[15] The (100) face is more open than the (111) face, and the corrugation can be expected to be higher for this face. However, it is expected that it should be of the same order of magnitude. Assuming a potential variation $8V_g=0.05$ eV gives a value $c\sim200$, and the expectation is that for K on Ni(100), c may in fact be substantially higher.

We find the minimum-energy configuration for (2) by shifting all atoms in the direction of the net force exerted on them. When the forces on all the atoms are zero, a minimum-energy configuration is reached. Numerically this is accomplished by moving each atom a distance proportional to the force exerted on it. The proportionality constant is adjusted to prevent a step so large that a move shoots past the minima and increases the energy. The process is terminated when the average force on the atoms falls below a preset tolerance, or the step size becomes reduced past a given limit. To ensure that the true minimum-energy configuration is attained, and not a local minima, the process is started from a variety of initial configurations.

The relaxation involves a hexagonal patch of 900 atoms. This patch is then extended using periodic boundary conditions so that the forces on the atoms at the edge of the patch can be calculated. A force cutoff radius of 40 (in the reduced units of a_0) is used to limit the range of the dipole-dipole interaction. The shape of the patch and the periodic boundary conditions are distorted appropriately so that a number of configurations in the coverage range 0.4–0.2 can be examined. The $c(3\times2)$ phase corresponds to a coverage of 0.33, and the $c(4\times2)$ phase has a coverage of 0.25.

It must be noted that the minimum in work function occurs for alkali metals adsorbed on fcc (100) at coverages around 0.25. Hence, the alkali-metal atoms in the uniaxial phase are in the metallization region of coverage identified by Persson and Ishida.[10] The model therefore is most accurate at the lower coverages considered.

III. RESULTS AND DISCUSSION

The influence of the substrate on the structure of the overlayer causes the adatoms to seek the $c(4\times2)$ configuration. Local patches where the adatoms have a $c(4\times2)$ registry are formed which are separated by domain walls. These domain walls have densities that are increased or decreased from the $c(4\times2)$ density depending on the imposed boundary conditions. Given the substrate alignment shown in Fig. 1, and unless the periodic boundary conditions are explicitly chosen to rotate the overlayer with respect to the substrate, the domain walls are always aligned parallel to the x (horizontal) and y (vertical) axis.

The nature of the domain wall depends on the interplay between alkali-metal atom interactions and interactions of the alkali-metal atoms with the substrate. The repulsive interaction between alkali-metal atoms seeks to place them in an equilateral triangular lattice. As shown in Fig. 1, the commensurate phases are distorted from forming a lattice of equilateral triangles. The resulting asymmetry causes the characteristics of the domain walls to differ with their alignment.

Providing the substrate corrugation is not too weak, a uniaxial phase with domain walls aligned only along the y axis is found to be the lowest-energy configuration at any given density. This configuration avoids placing an adatom on top of a substrate atom: the substrate interaction ranges between that of the minimum to that of the saddle point. If the substrate corrugation is weak, however, this configuration is not the lowest in energy.

A. Adlayer strain effects

If the substrate corrugation is too small, there is no reason for the alkali-metal atoms to form a uniaxial phase. Such a phase distorts alkali-metal atoms from forming a perfect equilateral triangular lattice. Consequently the alkali-metal interaction energy is increased at any given density by being forced to form a uniaxial phase. In the $c(4\times2)$ commensurate phase, the interaction between dipoles contributes an energy $0.540(2p^2/a_0^3)$ while the substrate interaction contributes $-4V_g$. For a perfect equilateral triangular lattice the dipole energy is $0.537(2p^2/a_0^3)$ and the substrate averages out to zero. For c values greater than 1500, the $c(4\times2)$ commensurate phase is not stable against a phase of uniform compression.

For high values of c, the $c(3\times2)$ configuration also forms a triangular lattice. The dipole energy is $0.834(p^2/a_0^3)$ while the substrate energy is $-2V_g$. For an equilateral triangular lattice at this density the dipole energy is $0.827(2p^2/a_0^3)$ and the substrate is zero. For c greater than 300, therefore, it is not energetically favorable to form a uniaxial phase at the $c(3\times2)$ density.

At densities between the $c(3\times2)$ and $c(4\times2)$ limits, a uniaxial phase is stable for c values much greater than that given by these two limits. At the density 0.289, the uniaxial phase has averaged atomic positions that form an equilateral triangular lattice. Consequently the dipole interactions are less stressed as the density approaches this limit. Away from this limit, however, if c is large, the alkali-metal atoms can be expected to deviate from a uniaxial configuration. The strain to the dipole interaction alone may explain the transition to rotated phases observed at increased densities.

B. Domain-wall characteristics

The positions of the atoms in the uniaxial phase can be specified in terms of displacements from the $c(4\times2)$ commensurate phase locations. The displacements produce only density modulations: There is no shearing of the positions of the atoms. Because of the orientation of the uniaxial phase, the positions of the atoms can be given as $x_i+u(x_i)$, where x_i is the location of the atom when they form a $c(4\times2)$ commensurate phase.

The values of $u(x)$ are shown in Fig. 2 when the uniaxial phase has a density of 0.254. The configurations are obtained with a c value of 10, 100, and 1000. For smaller values of c, there is clearly a strong modulation in the displacements of the atoms. For the most part, the atoms are in $c(4\times2)$ commensurate sites that are separated by increased density domain walls. The width of the domain wall is generally determined from the intercept of the tangent of $u(x)$ through the center of the domain wall with the continuation of the lines of commensurate spacings. At $c=10$, the domain wall has width $2a_0$, while at $c=100$ it is $7a_0$, and at $c=1000$ it is $18a_0$.

The average energy per atom $\bar{E}$ is also calculated. Plots of $\bar{E}a_0^3/2p^2$ as a function of the average area per atom A are shown in Fig. 3 for the values c of 10, 100, and 1000. These energy versus A relationships must be interpreted with the understanding that the dipole moment varies with density as well. The true energy per atom will reflect this change in the dipole moment, as well as changes in the holding potential of the substrate, V_0 in (1).

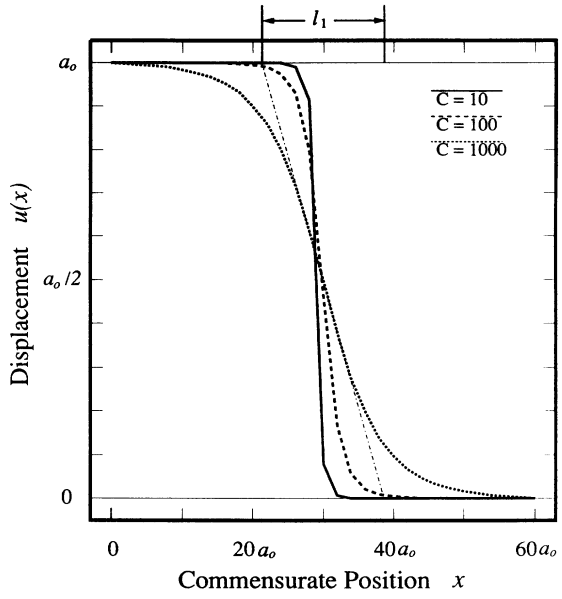

FIG. 2. The displacements of the atoms $u(x)$ from the commensurate position x for the cases $c=10$, 100, and 1000 when the uniaxial phase has density 0.254. The slope through the $c=1000$ curve is shown with the thin dash-dotted line. Its intercepts with the lines of commensurate spacing provide the domain-wall width l_1 shown.

It is interesting to note that the energy variation with A becomes linear in the $c(4\times2)$ commensurate limit value of 4. At $A=4$ there is a discontinuity in the slope. This behavior is consistent with the renormalized domain-wall concept proposed by Bak *et al.*[16] An energy

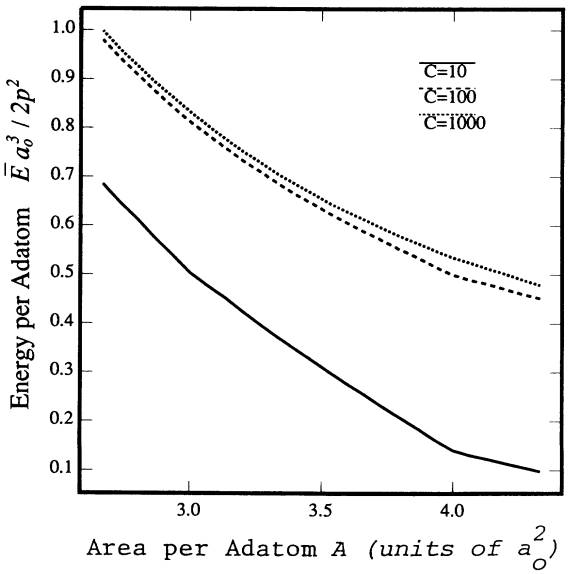

FIG. 3. Energy vs area per atom A for the cases $c=10$, 100, and 1000.

per length E_w can be assigned to the domain walls, and effective interactions can be identified between domain walls. In terms of the length unit a_0 the value of E_w is just the slope of the curves of Fig. 3 in the limit $A=4$ multiplied by $2p^2/a_0^4$. For $c=10$, the slope is 0.68 for $A<4$ and 0.26 when $A>4$. For $c=100$, the slopes are 0.52 and 0.28, respectively, while for $c=1000$ they are 0.44 and 0.34.

The change in slope at the $c(4\times2)$ commensurate density reflects the difference between domain walls of increased density and domain walls with depleted density. This change in slope is also noted at the $c(3\times2)$ commensurate density, $A=3$, in the $c=10$ curve. For $c=10$, the domain walls are so sharp that each domain wall can be considered to be a stripe of the $c(2\times2)$ commensurate with width a_0. At the $c(3\times2)$ density there is a change from having $c(4\times2)$ domains separated by $c(2\times2)$ domain walls, to having $c(2\times2)$ domains separated by $c(4\times2)$ domain walls.

At increased values of c, however, the atoms form a more regular triangular lattice. The configuration at $c(3\times2)$ does not stand out as being particularly more stable than the configurations at nearby densities. In fact, for a perfect triangular lattice on the substrate potential of (1), when half the atoms are at potential minima, the other half are at saddle points. Shifting the alkali-metal atoms uniformly in the x direction causes an increase in energy of the atoms at the minima, which is countered exactly by a decrease in energy of the atoms that occupied the saddle points.

The perfect $c(3\times2)$ configuration shown in Fig. 1, therefore, can be translated freely across the substrate. Two effects may stabilize this phase: significant higher-order terms which have been excluded from (1), or a decreased value of c leading to the configuration at the $c(3\times2)$ density being an alternating mix of $c(4\times2)$ and $c(2\times2)$ spacing. Such large variations in density associated with this type of $c(4\times2)$-$c(2\times2)$ structure will lead to a breakdown in the model as the alkali-metal atom interactions are modified from being simply interactions between dipole moments of uniform value. Should such large density variations actually occur, they will be evident in experimental scattering profiles.

C. Structure factors

Structure factors $S(\mathbf{q})$ are calculated at the density of 0.268, for configurations obtained with a value c of 10, 100, and 1000. The structure factor is obtained from $S(\mathbf{q})\approx|s(\mathbf{q})|^2$, where

$$s(\mathbf{q})=\sum_{\mathbf{r}_i} e^{i\mathbf{q}\cdot\mathbf{r}_i-r_i^2/40^2}, \tag{3}$$

the summation proceeds over the positions of the atoms which are extended via the periodic boundary conditions until the Gaussian weight factor falls below 2%. This Gaussian weight factor gives each structure factor peak the same amount of $\mathbf{q}$ Gaussian broadening. The height of the peak is proportional to the integrated peak intensity.

For a triangular lattice with basis vectors $\mathbf{R}_1=(0,a)$ and $\mathbf{R}_2=(-b,-a/2)$, the reciprocal-lattice vectors are generated from $\mathbf{q}_1=(-2\pi/b,0)$ and $\mathbf{q}_2=(\pi/b,2\pi/a)$. For the $c(4\times2)$ lattice, $a=2$ and $b=2$. For the lattice with density 0.268, $a=2$ and $b=1.87$. Structure factors are calculated as q_x is varied along the two lines $q_y=0$ and $q_y=2\pi/a$. These structure factors obtained at the density 0.268 when $c=10$, 100, and 1000 are shown in Fig. 4.

If the overlayer forms an undistorted triangular lattice, the peaks in the structure factor occur at integer multiples of $q_0=2\pi/b$ along the line $q_y=0$. Along the line $q_y=2\pi/a$, the main peaks are at $(n+\frac{1}{2})g_0$. These peaks, which are identified by capital letters, are clearly evident in Fig. 4 when $c=1000$. It is noted that the amplitudes of these peaks decrease as q_x varies away from 0. Small satellite peaks are also noted in the $c=1000$ plots. The location of peaks that would correspond to reciprocal-lattice vectors of the $c(4\times2)$ overlayer are identified by lower-case letters. For the configurations considered, only one such peak, e, is nonzero. This peak also corresponds to a reciprocal-lattice vector of the substrate.

When $c=100$, the satellite peaks shown in Fig. 4 are much stronger, reflecting an increased modulation in the

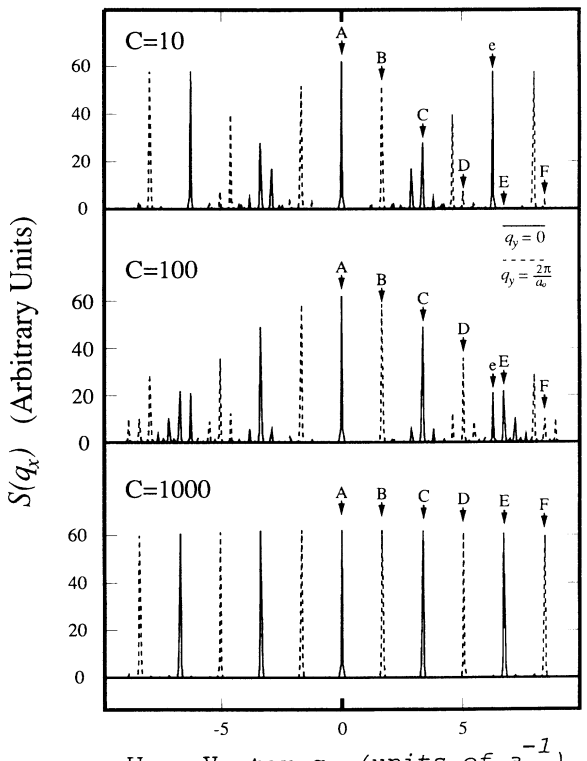

FIG. 4. Structure factors as a function of q_x calculated with $q_v=0$ (solid lines) and $q_y=(2\pi/a_0)$ (dashed lines) for the cases $c=10$, 100, and 1000 when the uniaxial phase has density 0.268. The location of the reciprocal-lattice peaks of the averaged triangular lattice are shown with capital letters. The location of the $c(4\times2)$ commensurate lattice peaks are shown with lower-case letters. Only one such peak, e, which is at a reciprocal-lattice vector of the substrate is nonzero.

positions of the atoms. Because the substrate is pulling the alkali-metal atoms to a $c(4\times2)$ commensurate lattice, the position of these peaks can be determined from the mismatch between the average lattice spacing of the atoms and the commensurate spacing. This mismatch, or misfit ϵ, is defined as

$$\epsilon=\frac{b_{4\times2}-b}{b_{4\times2}} , \tag{4}$$

with $b_{4\times2}=2$ when $b=1.87, \epsilon=0.067$. This misfit determines a length scale $L=a_0/\epsilon$ over which the structure of the alkali-metal atoms is repeated. The satellite peaks occur at q_x intervals of $2\epsilon q_0$ around the averaged triangular lattice peaks identified by capital letters in Fig. 4.

As the misfit is varied, the peaks shift in position. At the commensurate limit $\epsilon=0$ and all peaks coalesce at multiples of q_c. The amplitudes of the satellite peaks decrease away from the main peak, and they decrease as the misfit is increased. At increased misfits, the domain walls overlap more and the profile of the density modulation varies less sharply. This results in the reduced amplitude of the satellite peaks.

When $c=10$, the peak structure is changed radically. The satellite peaks around the B peak at $(q_0,0)$ are greatly increased in amplitude indicating the strong variation in the density modulation. The E peak, at $(2q_0,0)$, is completely absent, replaced by the peak e at $(2q_c,0)$. This peak e corresponds to a substrate adsorption site reciprocal-lattice vector and its amplitude being nearly equal to the amplitude of the A peak (0,0) indicates that all atoms are located close to adsorption sites.

D. Pinning and thermal effects

At low temperatures, the domain walls are not free to translate across the surface of the substrate. Because they are a collective structure of discrete adatoms, the energy of the domain wall varies with its position on the substrate.[17] Consequently a pinning energy E_p per domain-wall length is present. For the sine-Gordon soliton (appropriate to the weak substrate limit of our system),[18]

$$E_p=4\pi^2\lambda a_0 e^{-\pi^2\sqrt{\lambda/V}} , \tag{5}$$

where V is $2V_g/(Aa_0^2)$, the substrate corrugation divided by the area per adatom Aa_0^2, and the value λ can be obtained from the relationship of the ratio λ/V to the width of the domain wall l_1 in Fig. 2:

$$\frac{\lambda}{V}=\frac{l_1}{\pi a_0} . \tag{6}$$

Prokrosky and Talapov[19] have proposed that the depinning temperature should be

$$T_p\approx4\pi a_0\sqrt{\tilde{\lambda}E_p} , \tag{7}$$

where $\tilde{\lambda}$ is the line tension of the domain wall.

The line tension of the domain wall has commonly been assumed to be the energy per length as can be obtained from Fig. 3. However, as shown by Shrimpton and Joos,[20] the domain walls have string vibrations which do not alter the number of adatoms along their length. The appropriate value for the domain-wall line tension can be obtained from $\tilde{\lambda}=v^2\rho$, where v is the string wave velocity and ρ is its line density.

A phonon calculation similar to that for krypton on graphite[21] has been performed for the relaxed alkali-metal adatom configuration. A mode associated with string vibrations of the domain wall is identified and the string wave velocity is found to vary so that $v^2=(0.05/m)(2p^2/a_0^3)$ when the domain walls are reasonably broad. The mass per length of the domain wall can be determined from the wall profile.[22] For this system, the domain-wall density $\rho=0.32m/l_1$, where m is the mass of an alkali-metal atom and l_1 is the domain-wall width.

Consequently, for the alkali metals with dipole moments of several Debye, mass of the order of 100 amu, and domain walls $l_1\sim15a_0$, on a substrate with spacing $a_0\sim2.5$ Å, this gives a domain-wall line tension of the order of $\sim10^{-3}$ eV/a_0. This value can be compared to 0.8 eV/a_0, the energy per length of the domain wall obtained from Fig. 3.

Using (7) the depinning temperature will be roughly $10^4e^{-\pi l_1/(2a_0)}$ K. This is strongly dependent on the width of the domain wall. For $c=1000$, $l_1=18a_0$ and T_p is insignificant. For $c=100$, $l_1=7a_0$ and T_p is of the order of 1 K. With $c=10$, $l_1=2a_0$ and T_p is significantly increased. It should be noted, however, that the derivation for T_p assumes a broad domain-wall profile and hence a value at $c=10$ is not expected to be accurate.

Above the depinning temperature, the domain walls will vibrate as an elastic solid. Because the system is 2D, the vibrations will lead to a power-law shape of the structure-factor peaks.[23–25] Such line shapes depend on the temperature, the domain-wall elastic constants, and the position of the peak. Our calculation, which does not include thermal influences, does not give power-law line shapes; rather the finite-size cutoff conditions imposed on the structure-factor calculation give each peak a Gaussian profile. However, as shown by Dutta and Sinha,[26] the integrated intensity of the peaks will be insensitive to finite-size effects. Since our Gaussian profile peak values are proportional to the integrated peak area, the relative heights of the peaks will indicate the relative intensity associated with each peak regardless of the temperature.

IV. CONCLUSION

We call for high-resolution scattering studies of the uniaxial phase of alkali metals on the (100) surface. The relative peak intensities provide information through which the effective corrugation of the alkali-metal atom interaction with the metal surface can be determined.

If the ratio of the dipole interaction magnitude to the substrate corrugation magnitude, C, is greater than 1500, the alkali-metal atoms will not form a uniaxial phase as the coverage is increased from the $c(4\times2)$ density. With the alkali-metal dipole moments generally being of the order of a few Debye, the variation in the substrate potential must therefore be at least one-hundredth of an eV.

For such corrugations, the alkali atoms are only slightly displaced from a triangular lattice. The structure factor shows principal peaks which correspond to reciprocal-lattice vectors of this averaged triangular lattice.

If the substrate corrugation is of the order of a tenth of an eV, then anisotropy in the principal peak intensities should be noticed, as well as a decrease in principal peak intensity with increased wave vector. Satellite peaks should become apparent, mixed in with peaks which reflect the reciprocal-lattice vectors of the substrate. Domain-wall pinning will be a few degrees kelvin and should not be noticed at experimental temperatures.

For substrate corrugations of the order of a few tenths of an eV, the anisotropy, and decrease with wave vector of the averaged triangular lattice peaks, will be significant. The substrate peak at $(2q_c,0)$ will grow larger than the averaged triangular lattice peak at $(2q_0,0)$. The temperature of the domain-wall pinning will increase rapidly with substrate corrugation. Soliton glass phases similar to those found for the system of Pb on Cu(110) (Ref. 27) should be noticed at lower temperatures.

ACKNOWLEDGMENTS

We wish to acknowledge many useful discussions with R. Diehl, D. Fisher, and M. W. Cole. This work has been supported by NSF Grant No. DMR-8718771.

[1]R. D. Diehl, in *Phase Transitions in Surface Films,* edited by H. Taub, G. Torzo, H. Lauter, and S. C. Fain, Jr. (Plenum, New York, 1990).

[2]K. Muller, G. Besold, and K. Heinz, in *Alkali Adsorption on Metals and Semiconductors,* edited by H. P. Bonzel, A. M. Bradshaw, and G. Ertl (Elsevier, Amsterdam, 1989), p. 65.

[3]R. W. Gurney, Phys. Rev. **47**, 479 (1935).

[4]H. Ishida, Phys. Rev. B **42**, 10 899 (1990).

[5]D. M. Riffe, G. K. Wertheim, and P. H. Citrin, Phys. Rev. Lett. **64**, 57 (1990); C. Astaldi, P. Rudolf, and S. Modesti, Solid State Commun. **75**, 847 (1990).

[6]T. Aruga and Y. Murata, Prog. Surf. Sci. **31**, 61 (1989).

[7]K. Wandelt, in *Alkali Adsorption on Metals and Semiconductors* (Ref. 2), p. 25.

[8]R. L. Gerlach and T. N. Rhodin, Surf. Sci. **19**, 403 (1970).

[9]J. Topping, Proc. R. Soc. (London) Ser. A **114**, 67 (1927).

[10]B. N. J. Persson and H. Ishida, Phys. Rev. B **42**, 3171 (1990).

[11]T. L. Einstein, Langmuir **7**, 2520 (1991).

[12]A. G. Naumovets, Sov. Sci. Rev. A Phys. **5**, 443 (1984).

[13]L. M. Kahn and S. C. Ying, Surf. Sci. **59**, 333 (1976); see also E. Bauer, in *The Chemical Physics of Solid Surfaces and Heterogeneous Catalysis,* edited by D. A. King and D. P. Woodruff (Elsevier, Amsterdam, 1984), Vol. 3, p. 1.

[14]A. Zangwill, *Physics at Surfaces* (Cambridge University Press, Cambridge, 1989), p. 218.

[15]S. Chandavarkar and R. D. Diehl, Phys. Rev. B **38**, 12 112 (1988).

[16]P. Bak, D. Mukamel, J. Villain, and K. Wentowska, Phys. Rev. B **19**, 1610 (1979).

[17]S. Aubry, in *Solitons and Condensed Matter Physics,* edited by A. R. Bishop and T. Schneider (Springer-Verlag, London, 1979).

[18]V. L. Pokrovsky, A. L. Talapov, and P. Bak, in *Solitons,* edited by S. E. Trullinger, V. E. Zakharov, and V. L. Pokrovsky (North-Holland, Amsterdam, 1986), p. 71.

[19]V. L. Pokrovsky and A. L. Talapov, *Theory of Incommensurate Crystals* (Harwood Academic, New York, 1984).

[20]N. D. Shrimpton and B. Joos, Phys. Rev. B **40**, 10 564 (1989).

[21]N. D. Shrimpton and B. Joos, Phys. Rev. B **34**, 7334 (1986).

[22]N. D. Shrimpton and B. Joos, J. Phys. Condens. Matter **2**, 4099 (1990).

[23]S. N. Coppersmith, D. S. Fisher, B. I. Halperin, P. A. Lee, and W. F. Brinkman, Phys. Rev. B **25**, 349 (1982).

[24]A. Erbil, A. R. Kortan, R. J. Birgeneau, and M. S. Dresselhaus, Phys. Rev. B **28**, 6329 (1983).

[25]S. G. J. Mochrie, A. R. Kortan, R. J. Birgeneau, and P. M. Horn, Phys. Rev. Lett. **53**, 985 (1984).

[26]P. Dutta and S. K. Sinha, Phys. Rev. Lett. **47**, 50 (1981).

[27]K. S. Liang, K. L. D'Amico, C. H. Lee, and E. Y. Sheu, Phys. Rev. Lett. **65**, 3025 (1990).

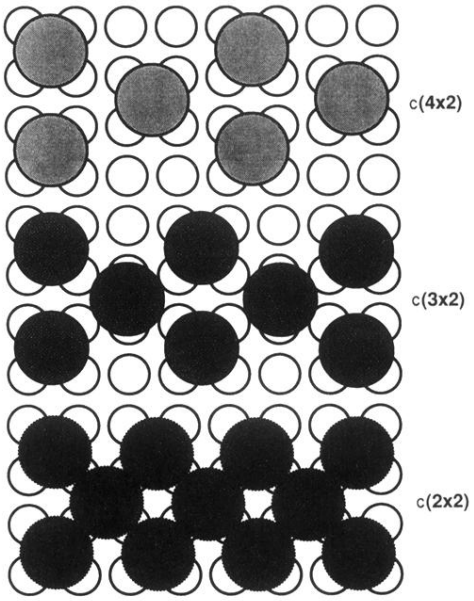

FIG. 1. The $c(4\times2)$, $c(3\times2)$, and $c(2\times2)$ commensurate phases.